12^{th} International Conference on Fracture Mechanics of Concrete and Concrete Structures
FraMCoS-12
B.L.A. Pichler, Ch. Hellmich, P. Preinstorfer (Eds)

https://doi.org/10.21012/FC12.1152
MS05-1:3

ON THE NUMERICAL MODELLING OF PUNCHING SHEAR IN FLAT REINFORCED CONCRETE SLABS BY MEANS OF THE FINITE ELEMENT METHOD

F. SUÁREZ*, J.C. GÁLVEZ†

*Departamento de Ingeniería Mecánica y Minera. Universidad de Jaén
Campus Científico-Tecnológico de Linares. Avda. de la Universidad (Cinturón Sur) – Linares, Spain
e-mail: fsuarez@ujaen.es

†Departamento de Ingeniería Civil-Construcción. Universidad Politécnica de Madrid
E.T.S.I. Caminos, Canales y Puertos, C/ Profesor Aranguren s/n - Madrid, Spain
e-mail: jaime.galvez@upm.es

Key words: Punching Shear, Cohesive Fracture, Finite Element Method

Abstract. The slab-column connection is a critical point in the design of a structure, mainly buildings, since a high concentration of shear stresses can lead to punching, which is a localised failure mode that can take place in a brittle manner and with no previous warning. Currently, structural standards provide recommendations and general expressions to help design these structural connections, where the Critical Shear Crack Theory (CSCT), proposed by Muttoni, stands out. This approach considers the shear strength as dependent on the crack width developing in the shear-critical region and uses a control perimeter (b_0) that delimits the cracking region. Many efforts have been devoted to understanding the failure mechanisms involved in punching and to propose tools, such as CSCT, for a safe and efficient design; nevertheless, there is still no consensus on the mechanics governing this phenomenon. The present contribution uses the finite element method and takes advantage of material models based on continuum damage mechanics to reproduce punching failure in reinforced concrete slabs. This approach is not new and has been employed in the past, but with limitations and some issues still not completely solved. The aim of this work is to analyse different possible modelling techniques in order to obtain a numerical model that reproduces this phenomenon with accuracy. A major advantage of using a finite element model in this case is that the main fracture mechanisms involved in the failure process, which are varied and complex, can be identified. Bidimensional and tridimensional models are discussed, and the possibility of taking into account the slip between concrete and the reinforcement bars, which turns out to be a key mechanism in the evolution of punching failure, is analysed.

1 INTRODUCTION

The slab-column connection in reinforced concrete structures is a critical point in structural design, especially in buildings, due to the high concentration of shear stresses that can lead to punching failure. This type of failure, characterized as a localized and brittle mechanism, occurs without prior warning and poses a considerable risk of partial structural collapse. The complexity of this phenomenon has driven various studies aimed at understanding and predicting the conditions under which punching failure occurs. From the experimental point of view the seminal work by Kinnunen and Nylan-

der can be highlighted [1]. In their experimental campaign, the fracture behaviour of slab-column connections with different reinforcement strategies was analysed, which helped to understand the role of the radial or concentric reinforcements, as well as to identify some failure mechanisms in the punching process. The work by Kinnunen and Nylander was later extended by Hallgren [2], where the punching problem using high strength concrete was analysed.

Together with the experimental work, some tools have been proposed to cope with the analysis and design of these structural connections. Among the most relevant approaches in this field is the Critical Shear Crack Theory (CSCT) proposed by Muttoni [3], which suggests that the shear capacity depends on the width of cracks developing in the shear-critical region. This theory uses a control perimeter (b_0) that defines the region where cracks are expected to develop, providing a valuable reference framework for slab-column connection design. Some other authors have approached punching failure by using analytical expressions [3–5], which may be convenient to provide structural engineers with easy to use tools that have been adopted by the standards [6, 7].

Despite theoretical and experimental advancements, there is still no consensus on the exact mechanisms governing punching. Some interesting works have used the finite element method to reproduce punching failure. For example, the works by Menétrey [8, 9] and Hallgren [2, 10] have contributed to understanding the phenomenon, though with limitations and aspects still unresolved.

In this context, the present work uses the finite element method (FEM) and material models based on continuum damage mechanics to reproduce punching failure in reinforced concrete slabs. Although this approach has been explored previously [9–11], challenges in its implementation persist, particularly regarding the modelling of the interaction between concrete and reinforcement bars, a key mechanism in the evolution of punching failure. This contribution analyses and compares different modelling techniques to develop a numerical model that accurately reproduces this phenomenon, thus facilitating the identification of the primary fracture mechanisms involved in the failure process.

2 EXPERIMENTAL BENCHMARK

2.1 Results by Kinnunen and Nylander

The experimental work carried out in [1] analyses punching failures using circular slabs with axial symmetry and includes a wide variety of specimens: with different column diameters, reinforcement ratios and reinforcement strategies (radial reinforcement, concentric reinforcement and orthogonal reinforcement). In this work the results have been obtained using specimen IA15a as reference. This slab has a diametre of 1840 mm, is supported on a 150mm diametre column; both, the column height and the slab thickness are equal to 150 mm. The reinforcement ratio is 0.8%.

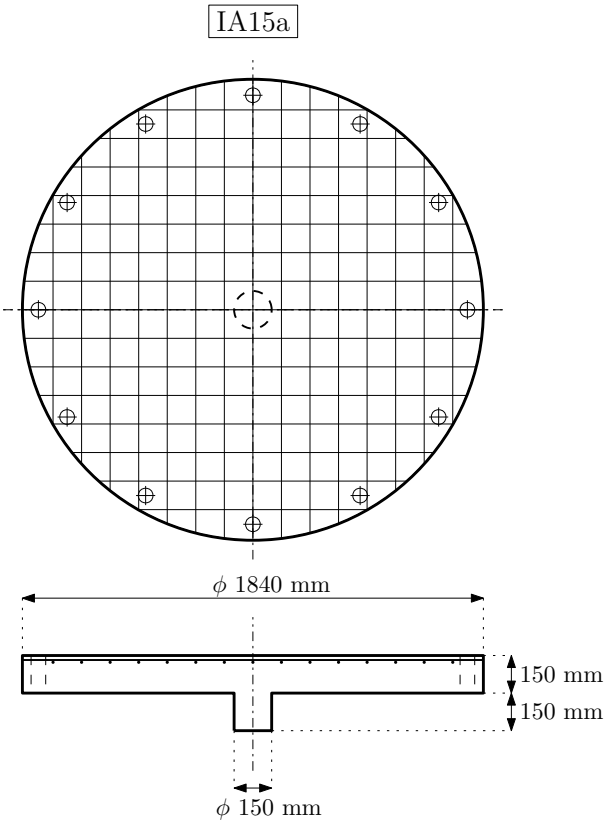

Figure 1: Main dimensions and reinforcement of IA15a specimens (plan and elevation views) [1]

The reinforcement is orthogonal and composed by 15 reinforcement bars in each of both perpendicular directions, all placed at the top of the slab. The main dimensions of the slab, as well as the reinforcement arrangements can be observed in Figure 1.

2.2 Experimental setup

Figure 2 shows a scheme of the experimental setup, which is numerically reproduced in this work. The load is applied by a hydraulic jack from below the specimen and the slab perimeter is retained by twelve tie rods and twelve spreader beams.

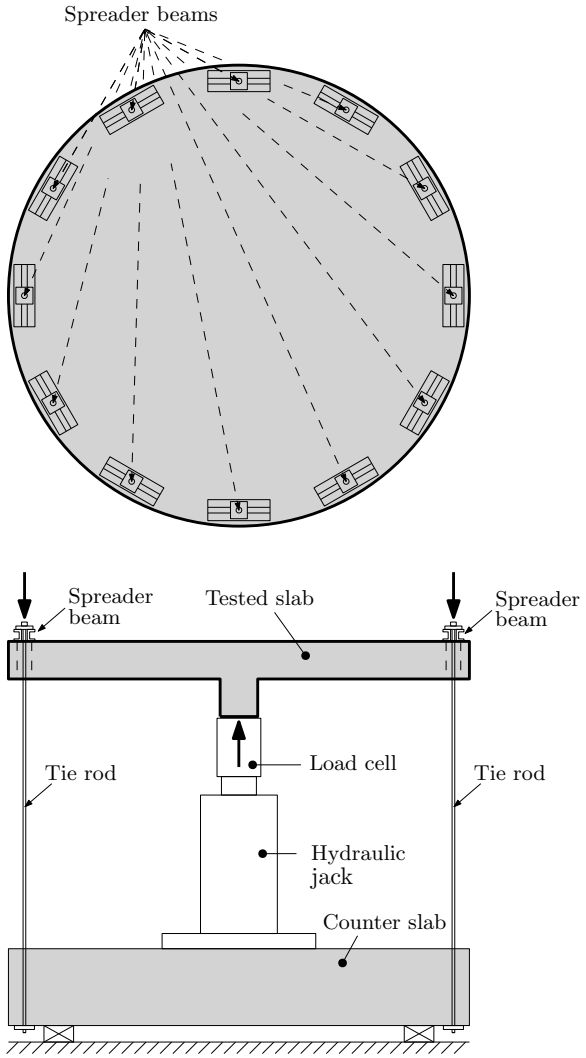

Figure 2: Experimental setup used in [1] (plan and elevation views)

The spreader beams help to distribute the perimeter load as uniformly as possible and the tie rods transmit the load to a counter slab placed a the bottom of the hydraulic jack.

3 NUMERICAL MODEL

To study the punching problem using the finite element method (FEM), three models have been prepared, all of them with the same boundary conditions, the same mesh and considering different possible contacts between the steel reinforcement and concrete. In this section, the characteristics of each of the three models are detailed. Regarding the mesh size, an initial analysis on the mesh was conducted and the mesh used here was deemed appropriate for the purpose of the study. The reference works [2, 8] employed coarser meshes and, in the context of what is analysed here, the influence of this aspect should not affect the main conclusions, provided that the same mesh is used for comparison.

In the following subsections, after the boundary conditions of the model are described, the material models used for each region of the slab are briefly presented and the characteristics of each of the three models are described.

3.1 Boundary conditions

The punching problem is modelled taking advantage of the axial symmetry and only one-sixtyfourth of the slab (a portion of 5.625 degrees around the symmetry axis). To reproduce the axial symmetry, the nodes at the bottom of the column are restricted in the vertical direction (z axis), the nodes at the symmetry axis are restricted in the radial direction (x axis) and the nodes at both radial planes are restricted in their perpendicular direction (see Figure 3).

3.2 Isotropic damage model for concrete

Fracture of concrete is reproduced using an isotropic damage formulation implemented in the open-source software OOFEM [12], a short description is provided here, although the complete description of the model can be found in the manuals of the software.

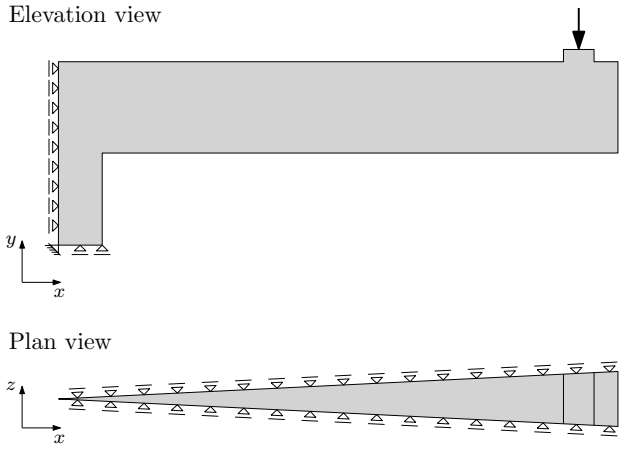

Figure 3: Boundary conditions of the FEM model.

Damage is numerically accounted for by means of the damage parameter ω, which ranges from 0 (no damage) to 1 (fully damaged) and reduces the material strength through the stiffness tensor by Eq. (1):

$$\boldsymbol{D} = (1-\omega)\,\boldsymbol{D}_e \tag{1}$$

where D_e stands for the elastic stiffness tensor.

Damage is obtained using an equivalent strain value, in this study the following expression, based on the Rankine criterion, is applied:

$$\varepsilon_{eq} = \frac{1}{E}\sqrt{\sum_{I=1}^{3}\langle\bar{\sigma}_I\rangle^2} \tag{2}$$

where $\bar{\sigma}_I$ represents the Ith principal stress and $\langle\cdot\rangle$ represents the Macauley brackets, thus only accounting for the positive principal stresses.

Damage evolution is defined by a stress-strain diagram that, in this case, has been described as exponential through Eq. (3).

$$\sigma = f_t \exp\left(-\frac{w}{w_f}\right) \tag{3}$$

where f_t stands for the concrete tensile strength, w is the crack opening at which σ is evaluated, and w_f is a parameter with the dimension of length (crack opening), that controls the shape of the exponential diagram (see Fig. 4). In fact, $w_f = G_f/f_t$, where G_f is the mode I fracture energy.

The model is formulated considering the crack band approach, so that w represents the crack opening that is equal to the inelastic strain ε_c, due to cracking, multiplied by the effective thickness h of the crack band. The value of h is estimated by projecting the finite element onto the direction of the maximum principal strain at the onset of damage, as suggested by Oliver [13].

Since the inelastic strain ε_c can be obtained as the difference between the total strain ε and the elastic strain σ/E:

$$\varepsilon_c = \varepsilon - \frac{\sigma}{E} = \varepsilon - (1-\omega)\varepsilon = \omega\varepsilon$$

Therefore, $w = h\varepsilon_c = h\omega\varepsilon$ and (3) can be rewritten as:

$$(1-\omega)E\varepsilon = f_t \exp\left(-\frac{h\omega\varepsilon}{w_f}\right)$$

which allows solving the value of damage ω for a specific value of strain ε.

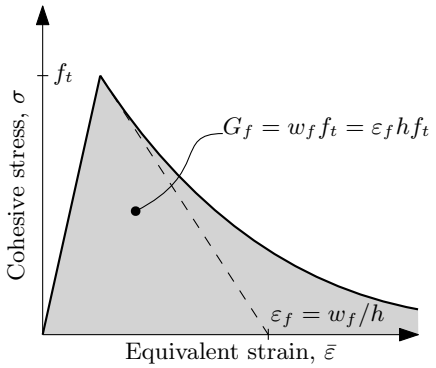

Figure 4: Exponential $\sigma - \bar{\varepsilon}$ diagram used to reproduce concrete fracture.

3.3 Perfectly plastic material for steel

In this work a simplified model for steel, usually adopted by the standards, is used. This model is elastic-plastic and its behaviour can be observed in Figure 5. The material behaves elastically up to a stress limit value f_y, which remains unchanged for greater strain values.

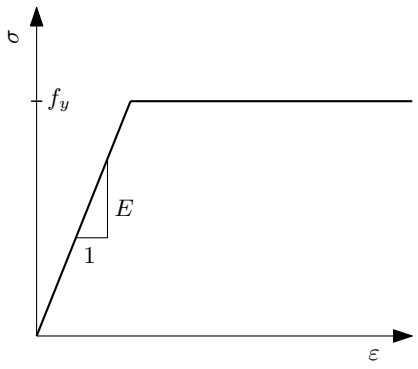

Figure 5: Elastic-plastic $\sigma - \varepsilon$ diagram used to reproduce steel behaviour.

3.4 Versions of the numerical model

Three versions of the finite element model have been used in order to analyse three strategies for modelling the punching failure problem. Schemes of models A, B and C can be observed in Figure 6; these models are described below.

3.4.1 Model A

In Model A, three materials are considered, with Material 1 corresponding to concrete and defined with the isotropic damage model described in Section 3.2, Material 2 corresponding to the region where the load is applied, defined as elastic and with the same elastic modulus as concrete, and Material 3 corresponding to steel and defined as perfectly plastic as described in Section 3.3. In this model no additional consideration is done regarding the concrete-steel contact, thus no debonding or slip between both materials are allowed. The characteristics of each material can be consulted in Table 1.

3.4.2 Model B

This model considers a perfect contact between concrete and steel with no bonding, therefore, steel bar can deform following the displacement of concrete but no tangential stresses appear between concrete and steel. To do this, steel is defined as additional elements that are overlapped with concrete. Those finite elements of concrete that overlap the position of the steel reinforcement are duplicated, forming a new set of elements that are defined as steel. The nodes of the elements of steel are *hanging nodes* that follow the position of the nodes of concrete only in the y direction, but moving freely in x and z.

To ensure the symmetry condition and the reinforcement anchorage at the perimeter of the slab, nodes at both ends of the reinforcement bar follow the concrete nodes they are related to in all directions, x, y and z.

Materials 1, 2 and 3 are defined exactly as in Model A.

3.4.3 Model C

This model is similar to Model B, thus steel is modelled as overlapping elements that, using *hanging nodes*, follow the displacement of the concrete elements to which they are related in the y direction, but not in the x and z directions, with the exception made in the extremes of the reinforcement bar, where steel nodes follow concrete nodes in all directions.

Unlike Model B, in this case the bonding between concrete and steel is taken into account. To do this, truss elements are defined along the concrete-steel contact, connecting each node in concrete with its corresponding hanging node of the steel bar; Figure 6c shows a scheme of this model, where the truss elements are represented as red springs.

In this work, these truss elements are defined with a cross section of 0.25 mm^2 and their material is defined as an isotropic damage model, described in Section 3.2, with the material characteristics shown in Table 1, where it is identified as Material 4.

Table 1: Material characteristics used in the FEM models

	E (MPa)	ν	f_t (MPa)	G_f (N/m)	f_y (MPa)
Material 1	25000	0.2	3	160	-
Material 2	25000	0.2	-	-	-
Material 3	210000	0.3	-	-	450
Material 4	25000	0.2	3	2000	-

a)

b)

c)

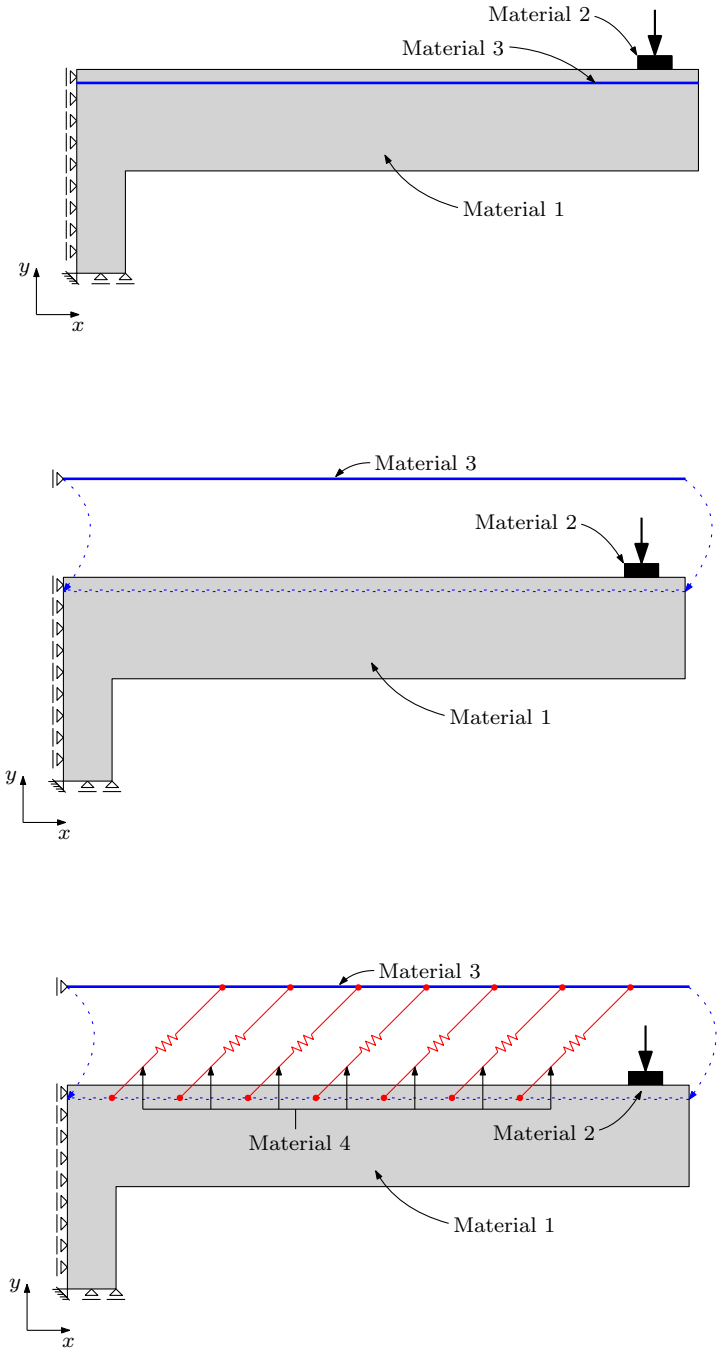

Figure 6: Schemes of the FEM model, a) Model A, b) Model B, c) Model C.

These elements and their material characteristics (Material 4) have not been specifically calibrated, as the aim here is to assess the influence of their inclusion on the overall behavior of the model. The calibration of these aspectas is left for future work.

This definition of the steel-concrete interface assumes a progressive debonding process between both materials and serves to understand how it affects the punching problem and the fracture mechanisms involved.

4 RESULTS

Figure 7 shows the load-displacement diagrams obtained with each of the three models described before.

It is worth noting that Model A, which does not consider the possible debonding between concrete and steel, shows a much more brittle behaviour than Models B and C, which allow relative displacement between both materials.

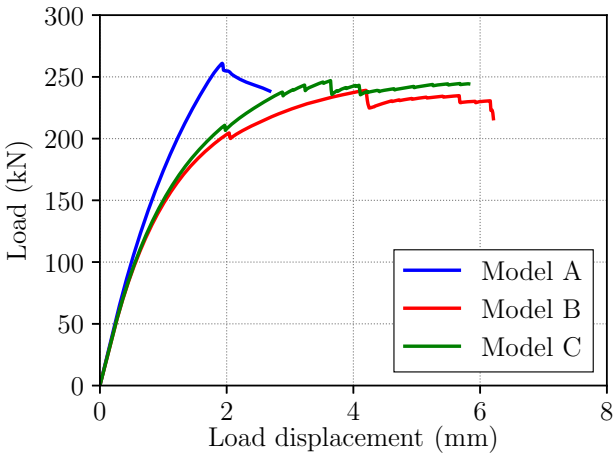

Figure 7: Load-displacement diagrams obtained with each of the models analysed.

Model A also presents a steeper initial branch, while models B and C show a more ductile and slightly more gradual load increase at the beginning of the load application.

Model B, which reproduces the extreme case where no tangential stresses are transmitted between concrete and steel, shows the most ductile behaviour of all three models and the least steep diagram. Regarding Model C, which represents an intermediate situation between Models A and B, since debonding between concrete and steel is allowed but certain tangential stresses are transmitted in the process, clearly presents an intermediate response between Models A and B.

Figure 8 shows map of damage in each of the models just before failure occurs. Note that these figures only show damage in the range of 0.95-1.00, with 1.00 corresponding to completely damaged material, in order to easily identified regions where damage is completely developed.

Damage in Model A develops in a completely different way compared with Models B and C. In Model A damage leads to early failure due to the fact that, since no slip is allowed between concrete and steel, small values of strain induces high damage in concrete while steel barely works and is not able to redistribute damage along the slab, thus leading to a very localised failure. This behaviour agrees with the works by Menétrey [8] and Hallgren [2]; an example of this is shown in Figure 9. In his work, Menétrey attributes this difference to the fact that this model is axisymmetric, which does not correctly represents the orthogonal geometry of the reinforcement.

Looking now at Model B, which represents the extreme case where debonding between concrete and steel is considered and no tangential stresses are transmitted between both materials, first cracking occurrence in concrete does not lead to failure, since the steel reinforcement is able to bear the tensile stresses induced by concrete cracking. In further stages of the loading process, damage extends further along the slab following the radial reinforcement position.

Finally, Model C, which represents a somehow more realistic case where the interface between concrete and steel can be damaged leading to debonding, shows a similar map of damage if compared with Model B, although interesting differences can be observed. On one hand, fracture progresses along the reinforcement alignment, although it is more limited than

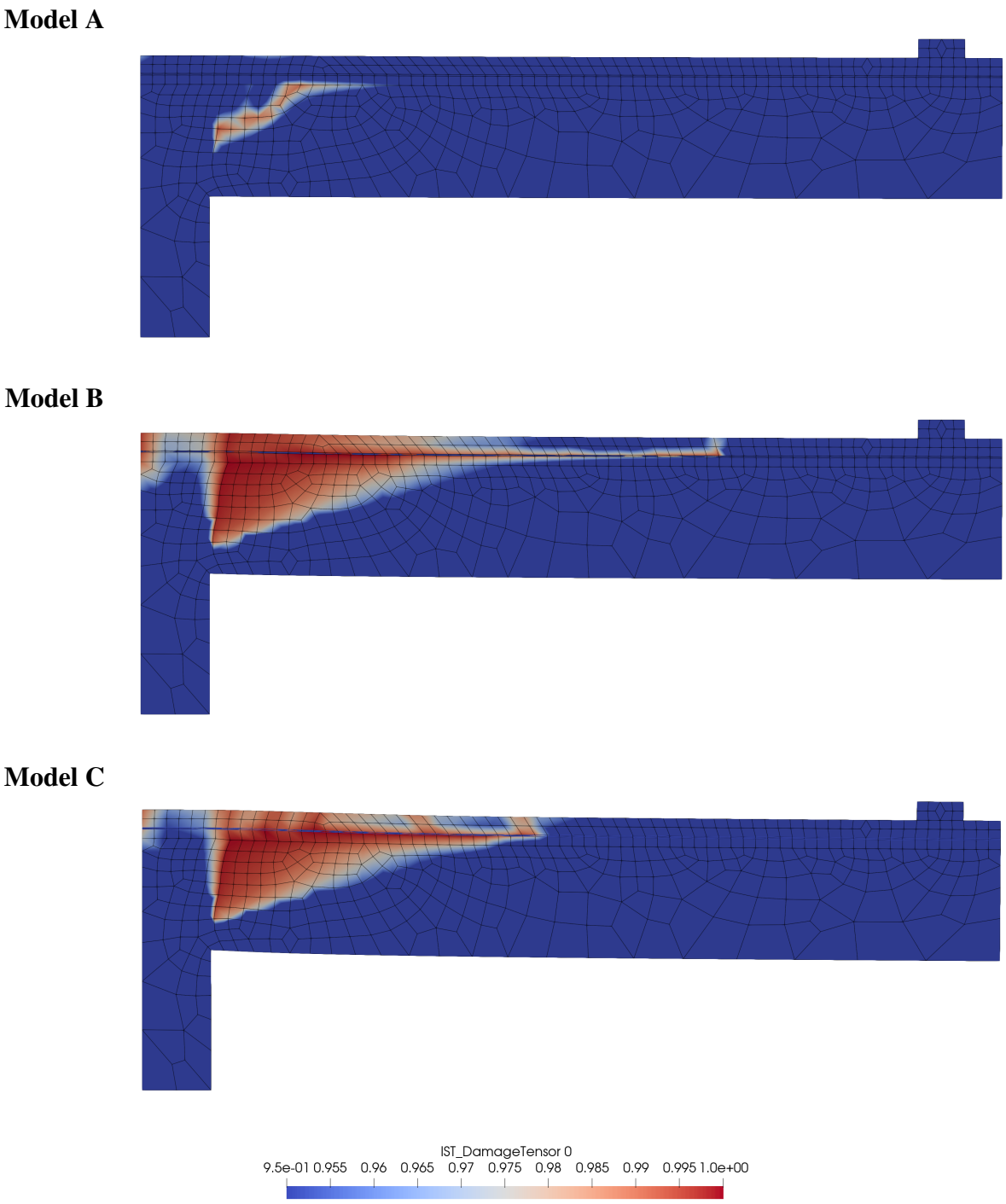

Figure 8: Color map of damage just before failure in each of the three analysed models.

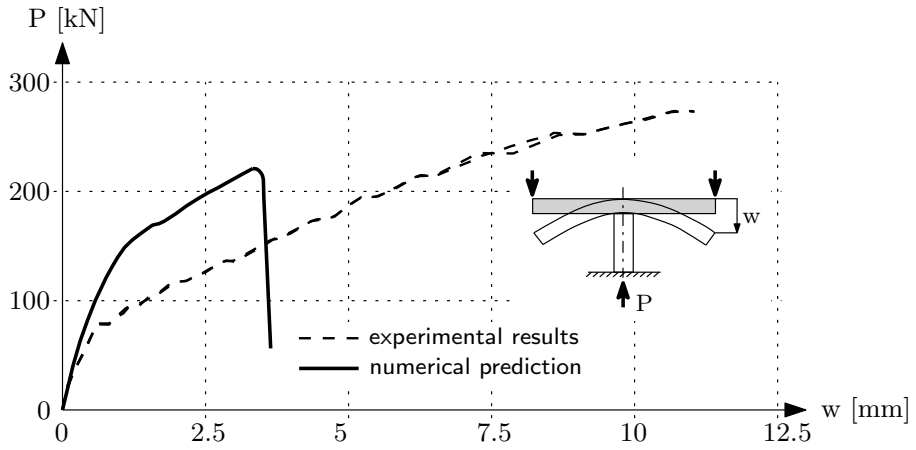

Figure 9: Comparison of the load-displacement diagrams obtained numerically and experimentally in a punching test in the work by Menétrey (extracted from [8]).

in the case of Model B. On another hand, failure process induces localized cracking on the top of the slab (five consecutive cracks can be observed in the figure), which are produced from the centre of the slab radially outwards.

The load-displacement diagrams in Figure 7 suggest that the stiffer behaviour of Model A in comparison with Models B and C is related to a more realistic representation of the concrete-steel interface.

5 CONCLUSIONS AND FUTURE WORK

- This work analyses punching failure using the finite element method and three approaches in the design of the model are utilised, highlighting the role of the steel-concrete interface in the failure mechanisms.

- When no debonding and slip is allowed between concrete and steel (Model A), failure occurs locally and at early stages of the test, with the response of the specimen being stiffer and more brittle than that observed experimentally.

- If the contact between concrete and steel allows slipping between both materials (Models B and C), failure extends to a wider region of the specimen, with a less stiff response in terms of the load-displacement diagram and presents a more ductile behaviour.

- The fracture parameters of the concrete-steel interface modify the overall ductility of the slab and modify the cracking pattern, inducing additional cracks on the surface of the slab.

- Future work may investigate on the influence of the fracture parameters of the interface to understand how to numerically reproduce its behaviour for a correct modelling of the problem.

ACKNOWLEDGEMENTS

The authors wish to acknowledge the financial support provided by the Ministry of Science, Innovation and Universities of Spain through the Research Fund Projects PID2023-149321OB-C31 and PID2023-149321OA-C33.

REFERENCES

[1] Kinnunen S, Nylander HSE. *Punching of concrete slabs without shear reinforcement.* Lindståhl. 1960.

[2] Hallgren M. *Punching shear capacity of reinforced high-strength concrete slabs.* Kungliga Tekniska Högskolan; 1996.

[3] Muttoni A. *Punching shear strength of reinforced concrete slabs without transverse reinforcement.* ACI structural Journal. 2008;**105(4)**:440-50.

[4] Koppitz R, Kenel A, Keller T. *Effect of punching shear on load–deformation behavior of flat slabs.* Engineering structures. 2014;**80**:444-57.

[5] Classen M, Kalus M. *Punching Shear Response Theory (PSRT)–A two degree of freedom kinematic theory for modeling the entire punching shear vs. deformation response of RC slabs and footings.* Engineering Structures. 2023;**291**:116197.

[6] Code A. Building code requirements for structural concrete (ACI 318-05) and commentary (ACI 318R-05). American Concrete Institute, Farmington Hills, Mich. 2005.

[7] Taerwe L, Matthys S, et al. *Fib model code for concrete structures 2010.* Ernst & Sohn, Wiley; 2013.

[8] Menétrey P. *Numerical analysis of punching failure in reinforced concrete structures.* EPFL; 1994.

[9] Menétrey P. *Synthesis of punching failure in reinforced concrete*. Cement and Concrete Composites. 2002;**24(6)**:497-507.

[10] Hallgren M, Bjerke M. *Non-linear finite element analyses of punching shear failure of column footings.* Cement and Concrete Composites. 2002;**24(6)**:491-6.

[11] de Sousa AM, Lantsoght EO, Genikomsou AS, Prado LP, Mounir K. *NLFEA of one-way slabs in transition between shear and punching: Recommendations for modeling.* Engineering Structures. 2023;**293**:116617.

[12] Patzák B. *OOFEM—an object-oriented simulation tool for advanced modeling of materials and structures.* Acta Polytechnica. 2012;**52(6)**.

[13] Oliver J. *A consistent characteristic length for smeared cracking models.* International Journal for Numerical Methods in Engineering. 1989;**28(2)**:461-74.